T-COM/35/6/14583

Spectral Correlation of Modulated Signals: Part II—Digital Modulation

W. A. Gardner
W. A. Brown, III
C.-K. Chen

Reprinted from: IEEE TRANSACTIONS ON COMMUNICATIONS, Vol. COM-35, No. 6, JUNE 1987

Spectral Correlation of Modulated Signals: Part II—Digital Modulation

WILLIAM A. GARDNER, SENIOR MEMBER, IEEE, WILLIAM A. BROWN, III, MEMBER, IEEE, AND CHIH-KANG CHEN, STUDENT MEMBER, IEEE

Abstract—**As a continuation of Part I, the spectral correlation function is presented for a variety of types of digitally modulated signals. These include digital pulse-amplitude, pulse-width, and pulse-position modulation, and various types of phase-shift keying and frequency-shift keying. The magnitudes of the spectral correlation functions are graphed as the heights of surfaces above a bifrequency plane, and these graphs are used as visual aids for comparison and contrast of the spectral correlation properties of different modulation types.**

I. Introduction

THIS paper is a continuation of Part I [1] where it is explained that the spectral correlation function is an important characteristic of modulated signals that can be exploited for various signal processing tasks such as detection, classification, parameter estimation and synchronization, and extraction, especially for signals buried in noise or masked by interference. In Part I, the spectral correlation function is calculated for the most commonly used types of analog modulation. In this Part II, the spectral correlation function is presented for a number of the most commonly used types of digital modulation, including digital pulse-amplitude, pulse-width, and pulse-position modulation, amplitude-shift keying, phase-shift keying (including BPSK, QPSK, SQPSK, and MSK), and coherent and incoherent frequency-shift keying. The magnitudes of the calculated spectral correlation functions are graphed as the heights of surfaces above the bifrequency plane in order to facilitate comparison and contrast of the spectral correlation properties of different modulation types. In the interest of brevity, the majority of details of the (sometimes tedious) calculations are omitted. The focus is on interpreting the general results for various special cases of practical interest.

The reader is reminded that in the graphs of the spectral correlation function, the surface above the f axis where $\alpha = 0$ is the conventional power spectral density function. This provides a benchmark against which the strength of spectral correlation can be measured. Also, because of the symmetries $\hat{S}_x^{\alpha}(-f) = \hat{S}_x^{\alpha}(f)$ and $\hat{S}_x^{-\alpha}(f) = \hat{S}_x^{\alpha}(f)^*$, only a quarter or a half of the bifrequency (f, α) plane is shown in some cases.

II. Digital Pulse Modulation

In a digitally modulated pulse train, with a digital signaling alphabet size of M, one of M distinct pulse types, say $\{q_1(t), q_2(t), q_3(t), \cdots, q_M(t)\}$, occurs every T_0 seconds, which can be expressed as

$$y(t) = \sum_{n=-\infty}^{\infty} \sum_{m=1}^{M} \delta_m(n) q_m(t - nT_0) \tag{1}$$

Paper approved by the Editor for Analog Communication of the IEEE Communications Society. Manuscript received October 21, 1985; revised October 30, 1986. This work was supported in part by the Naval Postgraduate School and in part by ESL, Inc.

The authors are with the Signal and Image Processing Laboratory, Department of Electrical and Computer Engineering, University of California, Davis, CA 95616.

IEEE Log Number 8714583.

where

$$\boldsymbol{\delta}(n) \triangleq [\delta_1(n), \delta_2(n), \delta_3(n), \cdots, \delta_M(n)]' \tag{2}$$

is an indicator vector (for each value of n) with one element equal to unity and the rest equal to zero. This signal can be interpreted as an M-vector PAM impulse train subjected to an M-vector time-invariant transformation (filter)

$$y(t) = q(t) \otimes x(t) \tag{3a}$$

where

$$x(t) = \sum_{n=-\infty}^{\infty} \boldsymbol{\delta}(n)\delta(t - nT_0) \tag{3b}$$

$$q(t) \triangleq [q_1(t), q_2(t), q_3(t), \cdots, q_M(t)]. \tag{3c}$$

Thus, the input–output spectral-correlation relation (24) in Part I [1] for multiple-input filters applies directly:

$$\hat{S}_y^{\alpha}(f) = Q(f + \alpha/2)\hat{S}_x^{\alpha}(f)Q'(f - \alpha/2)^* \tag{4a}$$

where

$$\hat{S}_x^{\alpha}(f) = \frac{1}{T_0}\tilde{S}_a^{\alpha}(f) \tag{4b}$$

and $\tilde{S}_{\delta}^{\alpha}(f)$ is the Fourier-series transform

$$\tilde{S}_{\delta}^{\alpha}(f) \triangleq \sum_{q=-\infty}^{\infty} \tilde{R}_{\delta}^{\alpha}(qT_0)e^{-i2\pi qT_0 f} \tag{5}$$

of the matrix of discrete-time cyclic autocorrelations

$$\tilde{R}_{\delta}^{\alpha}(qT_0) \triangleq \lim_{N\to\infty} \frac{1}{2N+1} \sum_{n=-N}^{N} \boldsymbol{\delta}(n+q)\boldsymbol{\delta}'(n) \cdot \exp[-i2\pi\alpha(n + q/2)T_0]. \tag{6}$$

Formula (4b) follows from the vector version of the spectral-correlation convolution relation (29) in [1], together with the spectral aliasing formula (27) in [1], and is simply the vector version of (48) in [1] with $Q(f) \equiv 1$.

For the special case in which $\{\boldsymbol{\delta}(n)\}$ is purely stationary, (4) reduces to

$$\hat{S}_y^{\alpha}(f) = \begin{cases} \frac{1}{T_0} Q(f + \alpha/2)\tilde{S}_{\delta}(f + \alpha/2)Q'(f - \alpha/2)^*, & \alpha = k/T_0 \\ 0, & a \neq k/T_0 \end{cases} \tag{7}$$

for all integers k (which is simply a vector version of the PAM formula (49) in [1]). Furthermore, if $\{\boldsymbol{\delta}(n)\}$ is an uncorrelated sequence and if the fraction-of-time distribution is uniform,

0090-6778/87/0600-0595$01.00

then

$$\tilde{R}_{\delta}^{\alpha}(qT_0)=\begin{cases}\dfrac{1}{M}I, & q=0,\ \alpha=k/T_0\\ \dfrac{1}{M^2}\mathbf{1}e^{-i\pi\alpha qT_0}, & q\neq 0,\ \alpha=k/T_0\\ 0, & \alpha\neq k/T_0\end{cases} \tag{8}$$

where I is the identity matrix and $\mathbf{1}$ is the matrix having all elements equal to unity. It follows from (8) that

$$\tilde{S}_{\delta}(f)=\left(\frac{1}{M}I-\frac{1}{M^2}\mathbf{1}\right)+\frac{1}{T_0M^2}\mathbf{1}\sum_{n=-\infty}^{\infty}\delta(f-n/T_0). \tag{9}$$

Substitution of (9) into (7) yields the explicit formula

$$\begin{aligned}\hat{S}_y^{\alpha}(f)=&\frac{1}{MT_0}\sum_{m=1}^{M}Q_m(f+\alpha/2)Q_m(f-\alpha/2)^*\\ &-\frac{1}{M^2T_0}\left[\sum_{m=1}^{M}Q_m(f+\alpha/2)\right]\left[\sum_{n=1}^{M}Q_n(f-\alpha/2)\right]^*\\ &\cdot\left[1-\frac{1}{T_0}\sum_{n=-\infty}^{\infty}\delta(f+\alpha/2-n/T_0)\right],\qquad \alpha=k/T_0.\end{aligned} \tag{10}$$

The cyclic spectra for a variety of digital pulse-modulated signals, such as pulse-position, pulse-width, and pulse-frequency modulation, can be obtained simply by substitution of the appropriate pulse transforms $\{Q_m(f)\}_1^M$ into (10) [or more generally into (7) or (4)].

Example (Pulse-Amplitude Modulation): Consider M-ary *pulse-amplitude modulation* (PAM) for which

$$Q_m(f)=a_mQ(f). \tag{11}$$

In this case, (10) reduces to (49) in [1], which reveals that the spectral correlation function is of the same general form for analog and digital PAM.

Example (Pulse-Position Modulation): Consider binary *pulse-position modulation (PPM)* for which $M = 2$ and

$$Q_m(f)=Q(f)e^{-i2\pi ft_m},\qquad m=1,\ 2 \tag{12}$$

for which $q(t)$ has nominal position zero. The spectral correlation magnitude surface from (10) for this signal is shown in Fig. 1 for $t_1/T_0 = 0$, $t_2/T_0 = 1/2$, and a rectangle pulse $q(t)$ starting at $t = 0$ with width $T_0/4$ [in Fig. 1(a)] and $T_0/2$ [in Fig. 1(b)]. The spikes represent impulses, and their heights are proportional to the areas of the impulses.

Example (Pulse-Width Modulation): Consider binary *pulse-width modulation* (PWM) for which $M = 2$ and

$$Q_m(f)=w_mQ(w_mf),\qquad m=1,\ 2 \tag{13}$$

for which $q(t)$ has nominal width unity. The spectral correlation magnitude surface from (10) for this signal is shown in Fig. 2 for rectangle pulses starting at $t = 0$ with widths $w_1 = T_0/2$ and $w_2 = T_0$ [in Fig. 2(a)] and $w_1 = T_0/4$ and $w_2 = T_0/2$ [in Fig. 2(b)].

III. Digital Carrier Modulation

Digital carrier-modulated signals can typically be expressed in the form of either PM/FM or QAM time series in which the amplitude- and/or phase- or frequency-modulating signals are digital pulse modulated. Thus, the formulas from the preceding section and [1] can be combined to obtain the spectral correlation formulas for these signal types. The most commonly employed digital carrier-modulated signals are either *amplitude-shift keyed* (ASK), *phase-shift keyed* (PSK), or *frequency-shift keyed* (FSK) signals, or combinations of

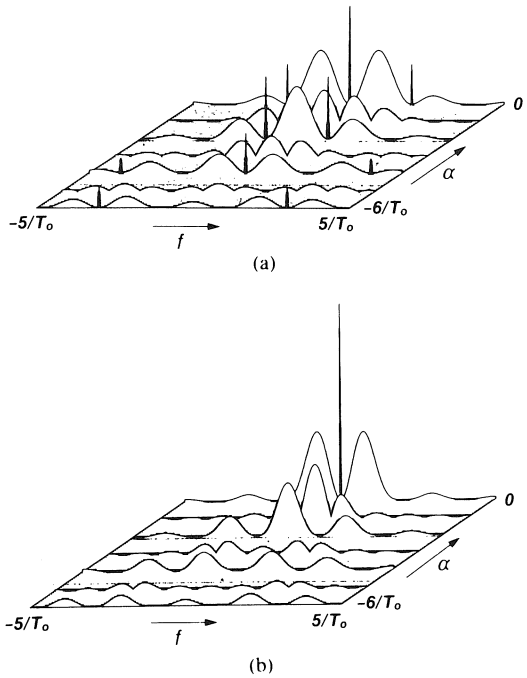

Fig. 1. Spectral correlation magnitude surfaces for a unity-power binary pulse-position modulated pulse train. (a) Pulse width = $T_0/4$, pulse positions = 0, $T_0/2$. (The strongest spectral-line power = 0.25.) (b) Pulse width = $T_0/2$, pulse positions = 0, $T_0/2$. (The strongest spectral-line power = 0.5.)

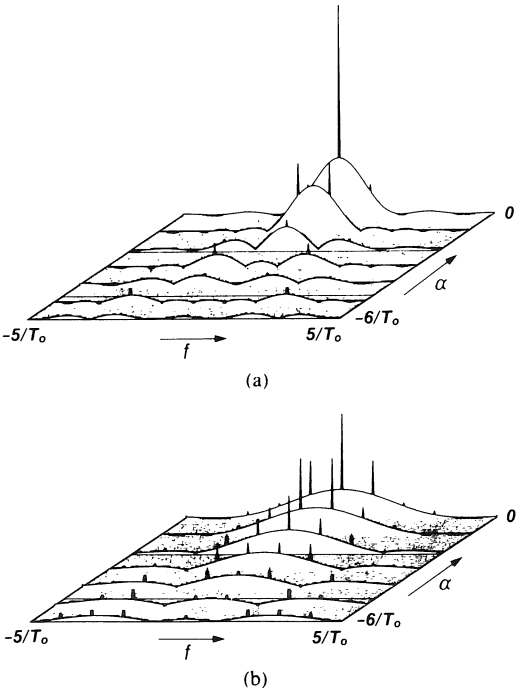

Fig. 2. Spectral correlation magnitude surfaces for a unity-power binary pulse-width modulated pulse train. (a) Pulse widths = $T_0/2$, T_0. (The strongest spectral-line power = 0.75.) (b) Pulse widths = $T_0/4$, $T_0/2$. (The strongest spectral-line power = 0.375.)

amplitude- and phase-shift keying (APK), or of phase- and frequency-shift keying.

A. Amplitude-Shift Keying

An ASK signal is simply an AM signal

$$x(t) = a(t)\cos(2\pi f_0 t + \phi_0) \tag{14}$$

in which the amplitude time series is a digital PAM signal

$$a(t) = \sum_{n=-\infty}^{\infty} a_n q(t - nT_0 - t_0). \tag{15}$$

Consequently, the spectral correlation function for an ASK signal is given by (40) in [1] with either (47) in [1] or (4) substituted for $\hat{S}_a^{\alpha}(f)$. For any alphabet size M, we obtain

$$\begin{aligned}\hat{S}_x^{\alpha}(f) = \frac{1}{4T_0}\{&[Q(f+f_0+\alpha/2)Q^*(f+f_0-\alpha/2)\tilde{S}_a^{\alpha}(f+f_0)\\ &+ Q(f-f_0+\alpha/2)Q^*(f-f_0-\alpha/2)\tilde{S}_a^{\alpha}(f-f_0)]e^{-i2\pi\alpha t_0}\\ &+ Q(f+\alpha/2+f_0)Q^*(f-\alpha/2-f_0)\tilde{S}_a^{\alpha+2f_0}(f)\\ &\cdot \exp[-i(2\pi[\alpha+2f_0]t_0+2\phi_0)]\\ &+ Q(f+\alpha/2-f_0)Q^*(f-\alpha/2+f_0)\tilde{S}_a^{\alpha-2f_0}(f)\\ &\cdot \exp[-i(2\pi[\alpha-2f_0]t_0-2\phi_0)]\},\end{aligned} \tag{16}$$

and for a full-duty-cycle rectangle pulse, we have

$$q(t) = \begin{cases} 1, & |t| \leq T_0/2 \\ 0, & |t| > T_0/2 \end{cases} \tag{17a}$$

and therefore

$$Q(f) = \frac{\sin(\pi f T_0)}{\pi f}. \tag{17b}$$

For a white amplitude sequence, we have

$$\tilde{S}_a^{\alpha}(f) = \begin{cases} \tilde{R}_a(0), & \alpha = k/T_0 \\ 0, & \alpha \neq k/T_0 \end{cases} \tag{18}$$

for all integers k. The spectral correlation magnitude surface specified by (16)–(18) for this ASK signal is shown in Fig. 3. If $f_0 T_0$ is sufficiently large to render negligible the overlap in the bifrequency plane of the four terms in (16), then ASK is, like PAM and AM, completely coherent for all f and α for which it is not completely incoherent and the power density is nonnegligible.

B. Phase-Shift Keying

A PSK signal is simply a PM carrier

$$x(t) = \cos[2\pi f_0 t + \phi(t)] \tag{19}$$

in which the phase time series is a digital PAM signal

$$\phi(t) = \sum_{n=-\infty}^{\infty} a_n q(t - nT_0 - t_0). \tag{20}$$

However, it is simpler to use the fact that a PSK signal is also a binary ASK signal for $M = 2$, and for $M > 2$, it is a QAM signal

$$x(t) = c(t)\cos(2\pi f_0 t + \phi_0) - s(t)\sin(2\pi f_0 t + \phi_0) \tag{21}$$

with digital PAM in-phase and quadrature components $c(t)$ and $s(t)$. Thus, for binary PSK (BPSK), the spectral correlation function is given by (16)–(17) (and for a white phase sequence, it is given by (16)–(18) with $\tilde{R}_a(0) = 1$).

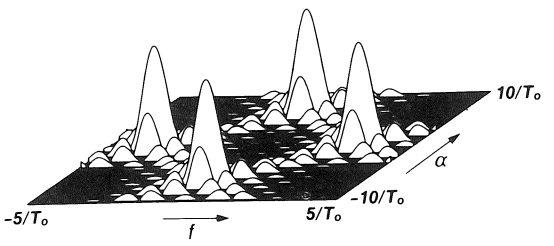

Fig. 3. Spectral correlation magnitude surface for amplitude-shift keying (and binary phase-shift keying) with carrier frequency = $3.3/T_0$.

For a quaternary PSK (QPSK) signal with phases separated by $\pi/2$ rad and with time-aligned in-phase and quadrature binary digital PAM signals

$$c(t) = \sum_{n=-\infty}^{\infty} c_n q(t - nT_0 - t_0)$$

$$s(t) = \sum_{n=-\infty}^{\infty} s_n q(t - nT_0 - t_0), \tag{22}$$

it can be shown that formula (67) in [1] with $\hat{S}_c^{\alpha}$ and $\hat{S}_s^{\alpha}$ each specified by (47) in [1] or (4) reduces to

$$\begin{aligned}\hat{S}_x^{\alpha}(f) = \frac{1}{2T_0}&[Q(f+\alpha/2+f_0)Q(f-\alpha/2+f_0)\tilde{S}_c^{\alpha}(f+f_0)\\ &+ Q(f+\alpha/2-f_0)Q(f-\alpha/2-f_0)\tilde{S}_c^{\alpha}(f-f_0)]e^{-i2\pi\alpha t_0}\end{aligned} \tag{23}$$

where $\tilde{R}_c(0) = \tilde{R}_s(0) = 1$ and for which it has been assumed that the in-phase and quadrature components are balanced in the sense that

$$\tilde{S}_c^{\alpha}(f) - \tilde{S}_s^{\alpha}(f) \equiv [\tilde{S}_{cs}^{\alpha}(f)]_r \equiv 0 \tag{24}$$

where $[\cdot]_r$ denotes the real part.

As a matter of fact, (23) applies to all APK signals that exhibit balanced amplitude-phase constellations. Specifically, if for every pair of amplitude and phase values, say (a_m, θ_m), there are the three additional pairs $(a_m, \theta_m + \pi/2)$, $(a_m, \theta_m + \pi)$, $(a_m, \theta_m - \pi/2)$, and if (for example) the sequence of amplitude-phase pairs is an uncorrelated purely stationary sequence with uniform fraction of time distribution, then (23)–(24) apply with

$$\tilde{S}_c^{\alpha}(f) = \begin{cases} \tilde{R}_c(0), & \alpha = k/T_0 \\ 0, & \alpha \neq k/T_0. \end{cases} \tag{25}$$

The spectral correlation magnitude surface for this class of balanced APK signals is shown in Fig. 4. Notice that in this class of APK signals, any number of amplitude values is allowed in the alphabet of amplitude-phase pairs; however, the number of phases must be an integer multiple of 4. If $f_0 T_0$ is sufficiently large to render negligible the overlap in the bifrequency plane of the two terms in (23), then these APK signals are completely coherent for all f and α for which they are not completely incoherent and the power density is nonnegligible. This includes only values of α that are integer multiples of the keying rate $1/T_0$. In contrast to the result for BPSK shown in Fig. 1, there is no spectral correlation associated with the carrier frequency f_0 (i.e., at $\alpha = \pm 2f_0 + k/T_0$) for balanced APK. It is balanced out between the in-phase and quadrature components. Also, unlike BPSK, there is no dependence of the spectral correlation on the carrier phase ϕ_0.

There are other types of PSK for which (23) does not apply because the in-phase and quadrature PAM signals are 50

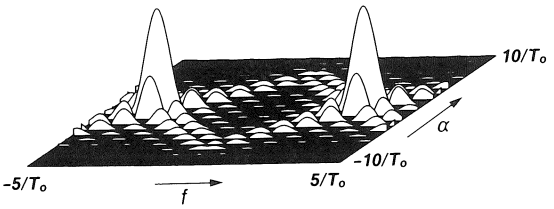

Fig. 4. Spectral correlation magnitude surface for balanced amplitude-phase-shift keying (and quaternary phase-shift keying) with carrier frequency = $3.3/T_0$.

percent staggered in time:

$$c(t)=\sum_{n=-\infty}^{\infty} c_n q(t-nT_0-t_0-T_0/2) \tag{26a}$$

$$s(t)=\sum_{n=-\infty}^{\infty} s_n q(t-nT_0-t_0). \tag{26b}$$

If it is assumed that $\{c_n\}$ and $\{s_n\}$ are statistically independent binary sequences with

$$\tilde{S}_{cs}^{\alpha}(f) \equiv 0, \tag{27}$$

then it can be shown using (67) in [1] and either (47) in [1] or (4) [for each of $c(t)$ and $s(t)$] that

$$\begin{aligned}\hat{S}_x^{\alpha}(f)=\frac{1}{4T_0}\{&Q(f+f_0+\alpha/2)Q^*(f+f_0-\alpha/2)\\ &\cdot[\tilde{S}_c^{\alpha}(f+f_0)e^{-i\pi\alpha T_0}+\tilde{S}_s^{\alpha}(f+f_0)]\\ &+Q(f+f_0+\alpha/2)Q^*(f-f_0-\alpha/2)\\ &\cdot[\tilde{S}_c^{\alpha}(f-f_0)e^{-i\pi\alpha T_0}+\tilde{S}_s^{\alpha}(f-f_0)]e^{-i2\pi\alpha t_0}\\ &+Q(f+\alpha/2+f_0)Q^*(f-\alpha/2-f_0)\\ &\cdot[\tilde{S}_c^{\alpha+2f_0}(f)e^{-i\pi(\alpha+2f_0)T_0}-\tilde{S}_s^{\alpha+2f_0}(f)]\\ &\cdot\exp[-i(2\pi[\alpha+2f_0]t_0+2\phi_0)]\\ &+Q(f+\alpha/2-f_0)Q^*(f-\alpha/2+f_0)\\ &\cdot[\tilde{S}_c^{\alpha-2f_0}(f)e^{-i\pi(\alpha-2f_0)T_0}-\tilde{S}_s^{\alpha-2f_0}(f)]\\ &\cdot\exp[-i(2\pi[\alpha-2f_0]t_0-2\phi_0)]\}.\end{aligned} \tag{28}$$

If $\{c(nT_c)\}$ and $\{s(nT_c)\}$ are statistically identical, purely stationary, uncorrelated sequences with zero means, then

$$\tilde{S}_c^{\alpha}(f)=\tilde{S}_s^{\alpha}(f)=\begin{cases}\tilde{R}_c(0), & \alpha=k/T_0\\ 0, & \alpha\neq k/T_0\end{cases} \tag{29}$$

and (28) reduces to

$$\hat{S}_x^{\alpha}(f)=\begin{cases}\dfrac{\tilde{R}_c(0)}{2T_0}[Q(f+\alpha/2+f_0)Q^*(f-\alpha/2+f_0)\\ \quad+Q(f+\alpha/2-f_0)Q^*(f-\alpha/2-f_0)]e^{-i2\pi\alpha t_0},\\ \quad\alpha=m/T_0,\ m \text{ even}\\ -\dfrac{\tilde{R}_c(0)}{2T_0}[Q(f+\alpha/2+f_0)Q^*(f-\alpha/2-f_0)\\ \quad\cdot\exp\{-i(2\pi[\alpha+2f_0]t_0+2\phi_0)\}\\ \quad+Q(f+\alpha/2-f_0)Q^*(f-\alpha/2+f_0)\\ \quad\cdot\exp\{-i(2\pi[\alpha-2f_0]t_0-2\phi_0)\}],\\ \quad\alpha=\pm 2f_0+m/T_0,\ m \text{ odd}\end{cases} \tag{30}$$

for this staggered QPSK (SQPSK) signal. A graph of the spectral correlation magnitude surface specified by (30) with $Q(f)$ given by (17) is shown in Fig. 5. It can be seen by comparison to Figs. 3 and 4 that SQPSK is similar to both BPSK and QPSK, yet distinct. Like BPSK, it does exhibit spectral correlation at *some* frequencies associated with the carrier frequency $\alpha = \pm 2f_0 + k/T_0$, but only for odd values of k. Like both BPSK and QPSK, it also exhibits spectral correlation at *some* frequencies associated with the keying rate alone $\alpha = k/T_0$, but only for even values of k. Also like BPSK, but unlike QPSK, there is some dependence on the carrier phase ϕ_0.

If the rectangle pulse shape $q(t)$ used in the SQPSK signal is modified to half a cycle of a sine wave,

$$q(t)=\begin{cases}\cos(\pi t/T_0), & |t|\leqslant T_0/2\\ 0, & |t|>T_0/2,\end{cases} \tag{31}$$

then this is called a *minimum-shift keyed* (MSK) signal. Formulas (28) and (30) still apply, but with

$$Q(f)=\frac{1}{2}[Q_0(f+1/2T_0)+Q_0(f-1/2T_0)] \tag{32}$$

where $Q_0(f)$is given by $Q(f)$ in (17). A graph of the spectral correlation magnitude surface specified by (30) and (32) is shown in Fig. 6.

As another illustration of the effect of a modification to the pulse shape used for PSK, we consider a BPSK signal with a bipolar pulse

$$q(t)=\begin{cases}1, & -T_0/2\leqslant t<0\\ -1, & 0\leqslant t<T_0/2.\end{cases} \tag{33}$$

This is sometimes called *Manchester-encoded* BPSK, whereas BPSK with the unipolar rectangle pulse (17) is called *nonreturn-to-zero* (NRZ) *encoded* BPSK. The spectral correlation magnitude surface for BPSK with pulse shape (33) is shown in Fig. 7.

C. Frequency-Shift Keying

One type of FSK signal is simply an FM carrier

$$x(t)=\cos(2\pi f_0 t+\int_0^t z(u)\,du) \tag{34a}$$

in which the instantaneous frequency-deviation time series is a digital PAM signal

$$z(t)=\sum_{n=0}^{\infty} a_n q(t-nT_0). \tag{34b}$$

Since the instantaneous phase of this signal is a continuous function of t (assuming that $q(t)$ contains no impulses), this is called *continuous-phase* FSK (CPFSK). The spectral correlation function for CPFSK can be obtained from (77) in [1] (for $\alpha = \pm 2f_0$). Another type of FSK, in which the phase is not necessarily continuous, can be expressed as

$$x(t)=\cos\left\{2\pi f_0 t+\sum_{n=0}^{\infty}\sum_{m=1}^{M}\delta_m(n)[2\pi f_m(t-nT_0)+\theta_m(n)]q(t-nT_0)\right\}. \tag{35}$$

If this signal is obtained by keying off and on M continuously running oscillators with frequencies $\{f_0 + f_m\}_1^M$, then

$$\theta_m(n)=2\pi f_m nT_0+\phi_m \tag{36a}$$

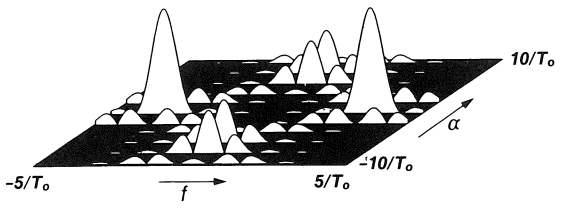

Fig. 5. Spectral correlation magnitude surface for staggered quaternary-phase-shift keying with carrier frequency = $3.3/T_0$.

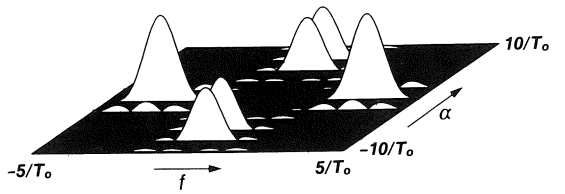

Fig. 6. Spectral correlation magnitude surface for minimum-shift keying with carrier frequency = $3.3/T_0$.

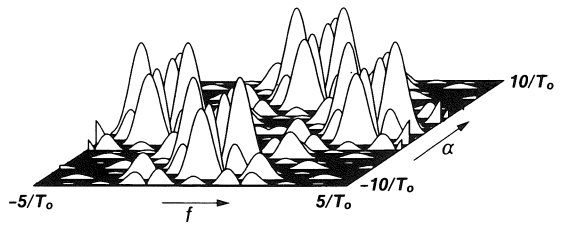

Fig. 7. Spectral correlation magnitude surface for Manchester-encoded binary phase-shift keying with carrier frequency = $3.3/T_0$.

and (35) reduces to

$$x(t)=\cos\left\{2\pi \sum_{n=0}^{\infty}\sum_{m=1}^{M} \delta_m(n)([f_0+f_m]t+\phi_m)q(t-nT_0)\right\} \tag{36b}$$

which is called *carrier-phase coherent* FSK. As an alternative, if the signal (35) is obtained by exciting M narrow-band filters with impulses every T_0 units of time, and if the filters are returned to the same initial state T_0 units of time after excitation, then

$$\theta_m(n)=\phi_m \tag{37}$$

in (35), and $x(t)$ is called *clock-phase coherent* FSK. In this case, each of the M possible carrier bursts of length T_0 always starts off with the same phase ϕ_m. If there are an integer number of carrier cycles per keying interval ($[f_0 + f_m]T_0$ = integer), then clock-phase coherence and carrier-phase coherence are equivalent. Also, if all M phases $\{\phi_m\}$ are equal and $[f_0 + f_m]T_0$ = integer, then (35) is a CPFSK signal (although CPFSK as generated in (34) does not require either clock-phase coherence or carrier-phase coherence unless $[f_0 + f_m]T_0$ = integer and $\{\phi_m\}$ are all equal). One other possibility is phase-incoherent FSK in which the phase sequence

$$\theta_m(n)=\theta_n \tag{38}$$

fluctuates randomly with n [and independently of $\delta_m(n)$].

Example (Clock-Phase Coherent FSK): Use of (37) in (35) yields the alternative but equivalent expression for the clock-phase coherent FSK signal:

$$x(t)=\sum_{n=0}^{\infty}\sum_{m=1}^{M} \delta_m(n)\cos\left(2\pi[f_0+f_m][t-nT_0]+\phi_m\right)q(t-nT_0) \tag{39}$$

where $q(t)$ is the rectangle pulse (17). This is a digital pulse-modulated signal (1) with

$$q_m(t)=\cos\left(2\pi[f_0+f_m]t+\phi_m\right)q(t). \tag{40}$$

Therefore, the spectral correlation function for this FSK signal is given by (7) (assuming the data $\{\delta(n)\}$ are purely stationary) with

$$Q_m(f)=\frac{\sin\left[\pi(f-f_0-f_m)T_0\right]e^{i\phi_m}}{2\pi(f-f_0+f_m)}+\frac{\sin\left[\pi(f+f_0+f_m)T_0\right]e^{-i\phi_m}}{2\pi(f+f_0+f_m)}. \tag{41}$$

If the data $\{\delta(n)\}$ are uncorrelated and have uniform fraction-of-time distribution, then (7) reduces to (10). Letting $f'_m = f_0 + f_m$, it follows that $|\hat{S}_x^{\alpha}(f)|$ has its maximum values at $\alpha = 0$ and $f = \pm f'_m$, and if $f'_m T_0$ are integers, then there are additional maxima at $\alpha = \pm 2f'_m$ and $f = 0$. There are also secondary maxima (down by the factor $M - 1$ from the primary maxima) at $\pm\alpha = f'_m \pm f'_n$ and $\pm f = (f'_m \mp f'_n)/2$.

Example (Phase-Incoherent FSK): The phase-incoherent FSK signal can be expressed in the alternative but equivalent form

$$x(t)=\sum_{n=0}^{\infty} a_n(t)q(t-nT_0) \tag{42a}$$

where

$$a_n(t)=\cos(2\pi[f_0+f(n)]t+\theta_n) \tag{42b}$$

and

$$f(n)=\sum_{m=1}^{M} \delta_m(n)f_m. \tag{42c}$$

If $\{\theta_n\}$ is an independent sequence, has uniform fraction-of-time distribution on the interval $[-\pi, \pi]$, and is statistically independent of $\{f(n)\}$, then it can be shown that the cyclic autocorrelation for this phase-incoherent FSK signal is given by the product

$$\hat{R}_x^{\alpha}(\tau)=\frac{1}{2T_0}\, r_q^{\alpha}(\tau)\tilde{M}_y^{\alpha}(\tau) \tag{43a}$$

where

$$r_q^{\alpha}(\tau)=\int_{-\infty}^{\infty} q(t+\tau/2)q(t-\tau/2)e^{-i2\pi\alpha t}\,dt \tag{43b}$$

and

$$\tilde{M}_y^{\alpha}(\tau)=\lim_{N\to\infty}\frac{1}{2N+1}\sum_{n=-N}^{N} y_n(\tau)e^{-i2\pi n\alpha T_0} \tag{43c}$$

for which

$$y_n(\tau) \triangleq \cos\left(2\pi[f_0+f(n)]\tau\right). \tag{44}$$

Thus, the spectral correlation function is given by the convolution (in the variable f)

$$\hat{S}_x^{\alpha}(f)=\frac{1}{2T_0}\left[Q(f+\alpha/2)Q^*(f-\alpha/2)\right] \otimes \int_{-\infty}^{\infty} \tilde{M}_y^{\alpha}(\tau)e^{-i2\pi f\tau}\,d\tau. \tag{45}$$

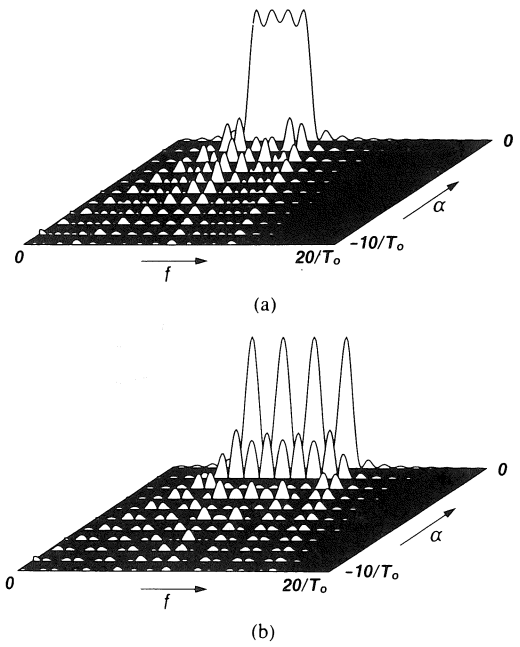

Fig. 8. Spectral correlation magnitude surfaces for phase-incoherent quaternary FSK. (a) $\{(f_0 + f_m)T_0\} = \{5, 6, 7, 8\}$. (b) $\{(f_0 + f_m)T_0\} = \{5, 7, 9, 11\}$.

If $\{f(n)\}$ is purely stationary and has discrete M-ary fraction-of-time distribution $\{P_m\}_1^M$, then it can be shown that

$$\tilde{M}_y^\alpha(\tau) = \sum_{m=1}^{M} P_m \cos(2\pi f'_m \tau), \qquad \alpha = k/T_0. \tag{46}$$

It follows from (45) and (46) that

$$\hat{S}_x^\alpha(f) = \frac{1}{4T_0} \sum_{m=1}^{M} P_m [Q(f+f'_m+\alpha/2)Q^*(f+f'_m-\alpha/2) + Q(f-f'_m+\alpha/2)Q^*(f-f'_m-\alpha/2)], \qquad \alpha = k/T_0. \tag{47}$$

Comparison of (10) (with (41) substituted in) to (47) reveals that some terms present in (10) are absent in (47), and as a result, there are no impulses in $\hat{S}_x^\alpha(f)$ for phase-incoherent FSK, unlike clock-phase coherent FSK, and there are no peaks at $\alpha = \pm 2f'_m$. In fact, if $2f'_m T_0$ is not an integer, there is no contribution at all at $\alpha = \pm 2f'_m$. However, if the products $\{f_m T_0\}$ are sufficiently large to render negligible the overlap in the bifrequency plane of the $2M$ terms in (47), then the incoherent-phase FSK signal (i.e., incoherent at the frequencies of the carrier bursts) is, to a close approximation, completely coherent (i.e., coherent at the clock rate and its harmonics) for all f and α for which any one of these $2M$ terms is nonnegligible. This includes only values of α that are integer multiples of the keying rate $1/T_0$. However, $f_m T_0$ is usually not very large in practice.

Two graphs of the spectral correlation magnitude surface specified by (47), corresponding to the two sets of frequencies $\{f'_m T_0\} = \{5, 6, 7, 8\}$ and $\{f'_m T_0\} = \{5, 7, 9, 11\}$ and a uniform distribution $P_m = 1/4$, are shown in Fig. 8.

IV. Conclusions

A new characteristic of modulated signals, the spectral correlation function, which is described in Part I [1], is calculated for a variety of digital modulation types. The results clarify the ways in which cyclostationarity is exhibited by different types of modulated signals. As explained in [1] and references therein, these differing spectral correlation characteristics can be used to empirically classify modulated signals, even when the signals are buried in noise, and they also can be exploited for signal detection, synchronization, and extraction. A signal can be synchronized to using a quadratic synchronizer if and only if it exhibits spectral correlation [4]. Similarly, the existence of spectral correlation in a signal of interest makes it possible to reject noise and interference for purposes of signal detection and extraction in ways that would be impossible for signals without spectral correlation [3], [5], [6]. The results in this paper are essential for design and analysis of signal processing systems such as detectors, classifiers, synchronizers, and extractors that exploit spectral correlation since one of the first steps in such design or analysis is to determine the spectral correlation characteristics of the signals of interest.

As explained in [1], the spectral correlation function reduces to the conventional power spectral density function for a cycle frequency of zero, $\alpha = 0$. Thus, the spectral correlation formulas derived herein yield the well-known formulas for power spectral density as a special case. A more extensive treatment of the spectral correlation characteristics of modulated signals that includes graphs of phase as well as magnitude is given in [3].

Acknowledgment

The authors gratefully acknowledge the interest of Prof. H. H. Loomis, Jr., and the resultant partial support of this work through the Naval Postgraduate School, and the interest of Dr. C. W. Scott, and the resultant partial support through ESL, Inc.

References

[1] W. A. Gardner, "Spectral correlation of modulated signals: Part I—analog modulation," *IEEE Trans. Commun.*, this issue, pp. 584–594.

[2] , *Introduction to Random Processes with Applications to Signals and Systems.* New York: Macmillan, 1985.

[3] , *Statistical Spectral Analysis: A Non-Probabilistic Theory.* Englewood Cliffs, NJ: Prentice-Hall, 1987, to be published.

[4] , "The role of spectral correlation in design and performance analysis of synchronizers," *IEEE Trans. Commun.*, vol. COM-34, Nov. 1986.

[5] W. A. Gardner, "Signal interception: A unifying theoretical framework for feature detection," in *Proc. Onzieme Colloque sur le Traitement du Signal et des Images,* Nice, France, June 1–5, 1987.
[6] W. A. Gardner and L. Paura, "Signal interception: Performance advantages of cycle detectors," in *Proc. Onzieme Colloque sur le Traitement du Signal et des Images,* Nice, France, June 1–5, 1987.

★

William A. Gardner (S'64–M'67–SM'84), for a photograph and biography, see this issue, p. 594.

★

William A. Brown, III (S'73–M'78) was born in Richland, WA, on February 13, 1952. He received the B.S. degree from California State University, Chico, in 1974 and the M.S. degree from the Illinois Institute of Technology, Chicago, in 1975, both in electrical engineering. He is currently a candidate for the Ph.D. degree in electrical engineering at the University of California, Davis.

From 1975 to 1977 he was a Teaching Assistant at Syracuse University, Syracuse, NY. From 1977 to 1981 he was a member of the Technical Staff at ARGOSystems, Sunnyvale, CA, working on passive sonar signal processing. Since 1981 he has been a Research Assistant at the University of California, Davis. His research interests include detection and estimation of random signals, adaptive filtering and beam forming algorithms, and signal processing hardware and software.

★

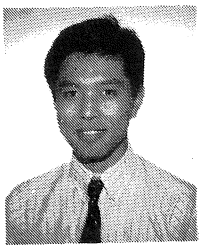

Chih-Kang Chen (S'81) was born in Shanghai, China, on June 15, 1959. He received the B.S. degree (with honors) in electrical engineering from California State University, Sacramento, and the M.S. degree in electrical engineering from the University of California, Davis, in 1983 and 1985, respectively.

He is currently pursuing the Ph.D. degree in electrical engineering at the University of California, Davis, where he is a Research Assistant. His research interests include statistical signal processing, system identification, and communications.

Mr. Chen is a member of Tau Beta Pi.